A Single Residue Differentiates between Human Cardiac and Skeletal Muscle Na^+ Channel Slow Inactivation

Yuriy Y. Vilin, Esther Fujimoto, and Peter C. Ruben
Department of Biology, Utah State University, Logan, Utah 84322 USA

ABSTRACT Slow inactivation determines the availability of voltage-gated sodium channels during prolonged depolarization. Slow inactivation in $hNa_V1.4$ channels occurs with a higher probability than $hNa_V1.5$ sodium channels; however, the precise molecular mechanism for this difference remains unclear. Using the macropatch technique we show that the DII S5-S6 p-region uniquely confers the probability of slow inactivation from parental $hNa_V1.5$ and $hNa_V1.4$ channels into chimerical constructs expressed in *Xenopus* oocytes. Site-directed mutagenesis was used to test whether a specific region within DII S5-S6 controls the probability of slow inactivation. We found that substituting V754 in $hNa_V1.4$ with isoleucine from the corresponding position (891) in $hNa_V1.5$ produced steady-state slow inactivation statistically indistinguishable from that in wild-type $hNa_V1.5$ channels, whereas other mutations have little or no effect on slow inactivation. This result indicates that residues V754 in $hNa_V1.4$ and I891in $hNa_V1.5$ are unique in determining the probability of slow inactivation characteristic of these isoforms. Exchanging S5-S6 linkers between $hNa_V1.4$ and $hNa_V1.5$ channels had no consistent effect on the voltage-dependent slow time inactivation constants [τ(V)]. This suggests that the molecular structures regulating rates of entry into and exit from the slow inactivated state are different from those controlling the steady-state probability and reside outside the p-regions.

INTRODUCTION

The excitability of skeletal and cardiac muscle is dependent upon the pool of available sodium channels as determined by fast and slow inactivation. Slow inactivation is structurally, pharmacologically, and kinetically distinct from fast inactivation (Chandler and Meves, 1970; Armstrong and Bezanilla, 1977; Rudy, 1978; Starkus and Shrager, 1978; Salgado et al., 1985; West et al., 1992; Catterall, 1993; Hartmann et al., 1994; Patton et al., 1992: Valenzuela and Bennett, 1994; Featherstone et al., 1996; Vedantham and Cannon, 1998). In contrast to fast inactivation, which develops in the millisecond time scale, slow inactivation operates in a time scale of seconds or tens of seconds (Ruff et al., 1988; Hille, 1992; Ruff, 1996; Wang and Wang, 1997), reflecting a unique physiological role for slow inactivation. Site-directed substitution of the structures necessary for fast inactivation, the IFM motif, does not prevent slow inactivation (Featherstone et al., 1996).

Studies have demonstrated that slow inactivation contributes to the activity of voltage-gated sodium channels by regulating membrane excitability, firing properties, and spike frequency adaptation (Ruff et al., 1988; Sawczuk et al., 1995; Fleidervish et al., 1996). It has also been proposed that slow processes in sodium channel inactivation might be a molecular memory mechanism that preserves traces of previous activity (Toib et al., 1998).

Received for publication 15 December 2000 and in final form 16 February 2001.

Address reprint requests to Dr. Peter C. Ruben, Department of Biology, Utah State University, 5305 Old Main Hill, Logan, UT 84322-5305. Tel.: 435-797-2490; Fax: 435-797-1575; E-mail: pruben@biology.usu.edu.

0006-3495/01/05/2221/10 $2.00

The properties of slow inactivation differ among sodium channel isoforms. We and others have previously shown that slow inactivation in cardiac sodium channels ($hNa_V1.5$) (see Goldin et al., 2000) is less extensive and has slower rates than skeletal muscle ($hNa_V1.4$) sodium channels (Townsend and Horn, 1997; Richmond et al., 1998; O'Reilly et al., 1999). Because of its greater probability, slow inactivation in $hNa_V1.4$ channels might have a significant role in skeletal muscle fatigue (Ruff et al., 1988). In contrast, less extensive slow inactivation in $hNa_V1.5$ channels may prevent the potential rundown of cardiac muscle excitability during repetitive contractions under normal physiological conditions.

Sodium channels have been cloned and the primary structure sequenced. These channels consist of a large α-subunit (230–270 kDa) and smaller (37–39 kDa) β-subunits (Rogart et al., 1989; Trimmer et al., 1989; George et al., 1992; Gellens et al., 1992; also see the review by Fozzard and Hanck, 1996). The α-subunit consists of four homologous domains (DI–DIV), and each domain contains six transmembrane segments (S1–S6). The domains are arranged in a ring-shaped structure with the ion permeation pathway in the center, which is believed to be formed by the S5-S6 extracellular linkers (p-regions) of each domain (Sato et al., 1998). A number of reports indicate the importance of p-regions in regulating slow inactivation (Cummins and Sigworth, 1996; Hayward et al., 1997; Makita et al., 1996; Wang and Wang, 1997) in sodium channels. $hNa_V1.4$ and brain sodium channels require the co-expression of β_1-subunit for normal gating (Isom et al., 1992; Cannon et al., 1993; Yang et al., 1993; Isom et al., 1994; Patton et al., 1994; Chen and Cannon, 1995), whereas the functional role of the β_1-subunit in $hNa_V1.5$ channels is less clear (Makita et al., 1994; McCormick et al., 1998). Co-expression of the

β_1-subunit with $hNa_V1.4$ channels stabilizes slow inactivation but has only a subtle effect on slow inactivation in $hNa_V1.5$ channels (Vilin et al., 1999). Thus, although these studies provide some information about the molecular underpinnings of slow inactivation in sodium channels, the precise mechanism of this biophysical process still remains unclear.

Because the p-region structure of $hNa_V1.4$ α-subunit differs from that of $hNa_V1.5$ (Trimmer et al., 1989; George et al., 1992; Rogart et al., 1989; Gellens et al., 1992), we previously explored whether transposing all four $hNa_V1.5$ S5-S6 extracellular linkers into a $hNa_V1.4$ backbone would confer $hNa_V1.5$-like steady-state slow inactivation probability to the chimerical construct (Vilin et al., 1999, 2000). Our results indicated that isoform-specific structural differences in one or more S5-S6 linkers underlie at least some of the properties of slow inactivation that differ between $hNa_V1.4$ and $hNa_V1.5$ channels.

The goal of the present study was to more precisely account for the differences in slow inactivation between $hNa_V1.4$ and $hNa_V1.5$ channels by using $hNa_V1.4$/$hNa_V1.5$ channel chimeras with individually interchanged S5-S6 linkers from domains DI, DII, DIII, and DIV. Our results show non-equivalent contributions of single S5-S6 linkers in slow inactivation; the S5-S6 linker in domain II, but not in I, III, and IV, is crucial in controlling the steady-state probability of slow inactivation in both $hNa_V1.4$ and $hNa_V1.5$ sodium channels. We also show that swapping a single residue in domain II S5-S6 linker produces isoform-specific probabilities of steady-state slow inactivation in the mutated $hNa_V1.4$ and $hNa_V1.5$ sodium channels. We have therefore pinpointed, to the level of a single amino acid residue, the structural difference underlying the difference in slow inactivation probability between cardiac and skeletal muscle sodium channels.

MATERIALS AND METHODS

Molecular biology

$hNa_V1.4$ and $hNa_V1.5$ sodium channels were constructed as previously described (Featherstone et al., 1996; Richmond et al., 1998). Chimeras were constructed as follows. The domain II pore region in $hNa_V1.5$ (residues 863–913) was replaced with the domain II pore region from $hNa_V1.4$ (residues 724–776, here called CSk2). The domain III pore region in $hNa_V1.5$ (residues 1359–1443) was replaced with the domain III pore region from $hNa_V1.4$ (residues 1185–1268, here called CSk3). In CP13, hH1 residues 864–871 were replaced with 725–734 of $hNa_V1.4$. In CP15, hH1 residues 864–887 were replaced with 725–750 of $hNa_V1.4$. Chimeras were prepared using a modified, three-fragment polymerase chain reaction (PCR) overlap extension method (Ho et al., 1989). For each clone, a set of six primers was used, four primers at the junctions of $hNa_V1.5$ and $hNa_V1.4$ and two outer primers, in combination with the appropriate template cDNA, hHla/pGEM3Z or $hNa_V1.4$/pSP64T. The chimeric full-length PCR fragment was prepared by overlapping the first two fragments, an $hNa_V1.5$ and an $hNa_V1.4$ fragment, and then overlapping this fragment with the third $hNa_V1.5$ fragment in a separate amplification reaction. For CSk2, CP13, and CP15, an *Eco*RI-*Sma*I fragment was replaced; for CSk3, a *Nde*I-*Bst*EII fragment was replaced. The mirror chimeras, in which pore regions from $hNa_V1.5$ were transposed into $hNa_V1.4$, were constructed as previously described (Makita et al., 1996). Specifically, these chimeras included domain II p-region from $hNa_V1.5$ transposed into $hNa_V1.4$ (here called SkC2) and the domain III p-region from $hNa_V1.5$ transposed into $hNa_V1.4$ (SkC3). Finally, p-regions from domains I and IV were transposed from $hNa_V1.5$ (residues 277–390 and 1683–1747) into $hNa_V1.4$ (residues 277–424 and 1508–1573, here called SkC14), and p-regions from domains I and IV were transposed from $hNa_V1.4$ into $hNa_V1.5$ (called CSk14). The structure of all chimeras used in this study is shown in Figs. 1 and 3. Other mutations, including I891V, V754I, and A773S/A776S, were prepared with a two-fragment PCR overlap extension. Equal volumes of α-mRNA (1 μg/μl) and β-mRNA (2 μg/μl) were mixed together before injection.

Oocyte preparation and RNA injections

Stage V-VI oocytes were surgically removed from female *Xenopus laevis* (Nasco, Modesto, CA), enzymatically isolated, and maintained in culture for up to 14 days at 18°C as described (Vilin et al., 1999). Approximately 24 h after enzymatic treatment oocytes were individually injected with 27 nl of mRNA, using a Drummond automatic injector. Before macropatch recording, the vitelline membrane was manually removed from oocytes after a short (2–3 min) exposure to a hyperosmotic solution containing (in mM): 96 NaCl, 2 KCl, 20 $MgCl_2$, 5 HEPES, 400 mannitol, pH 7.4.

Electrophysiology

All macropatch recording was done in a chamber containing (in mM): 9.6 NaCl, 88 KCl, 11 EGTA, 5 HEPES, pH 7.4. This solution was intended to zero the oocyte membrane potential. Aluminosilicate patch electrodes were pulled on a Sutter P-87 (Sutter Instruments, Novato, CA), dipped in melted dental wax to reduce capacitance, thermally polished, and filled with (in mM): 96 NaCl, 4 KCl, 1 $MgCl_2$, 1.8 $CaCl_2$, 5 HEPES, pH 7.4. Electrophysiological recordings were made using an EPC-9 patch-clamp amplifier (HEKA, Lambrecht, Germany), and digitized at 200 kHz via an ITC-16 interface (Instrutech, Great Neck, NY). Voltage clamping and data acquisition were controlled via Pulse software (HEKA) running on a G4 Power Macintosh. All data were software-low-pass filtered at 5 kHz during acquisition. Experimental bath temperature was maintained at 22 ± 0.2°C for all experiments using a Peltier device controlled by an HCC-100A temperature controller (Dagan, Minneapolis, MN). After seal formation, patches were left on-cell for all recordings. Holding potential for all experiments was −100 mV. Leak subtraction was performed automatically by the software using a p/4 protocol before the test pulse. Leak pulses alternated in direction from a holding potential of −120 mV.

Data analysis

Analysis and graphing were done using PulseFit (HEKA) and Igor Pro (Wavemetrics, Lake Oswego, OR), both run on a G4 Power Macintosh. Time constants (τ) for onset and recovery of fast and slow inactivation were derived from single-exponential fitting to peak current amplitude versus prepulse (or interpulse) duration using the following equation:

$$I = I_{SS} + a_1 \exp(-t/\tau), \quad (1)$$

where I is current amplitude, I_{SS} is the steady-state current or asymptote (plateau amplitude), a_1 is the amplitude at time $t = 0$ (time of peak current), and τ is the time constant (Vilin et al., 1999).

Steady-state slow inactivation data were fitted with a modified Boltzmann function:

$$I/I_{max} = (I_1 - I_2)/[(1 + \exp(-ze_o(V_m - V_{1/2}))/(kT)] + I_2 \quad (2)$$

where I_{max} is the maximum peak current measured, I_1 and I_2 are the maximum and minimum values in the fit, V_m is the prepulse potential, $V_{1/2}$ is the midpoint voltage of the steady-state slow inactivation curve, e_o is an elementary charge, z is apparent valence (slope factor), k is the Boltzmann constant, and T is absolute temperature. The maximum probability of slow inactivation was measured as I/I_{max} at the most depolarized voltage of the steady-state curve. For brevity, we refer to the maximum probability of steady-state slow inactivation as, simply, probability of slow inactivation.

All statistical values, both in the text and in the figures, are given as means ± SEM. Exponential or Boltzmann fits were performed for each individual data set to obtain mean ± SEM for the time constants, $V_{1/2}$, and z. Statistical differences were derived from Student's t-test or, where indicated, Welch alternate t-test, with two-tailed p values using the Instat software package (GraphPad Software, San Diego, CA).

RESULTS

S5-S6 linkers in domain II determine the probability of slow inactivation in $hNa_V1.4$ and $hNa_V1.5$ channels

Several lines of research have suggested that slow inactivation gating in sodium channels may involve the conductance pathway. We therefore sought to elucidate the role of the p-regions (S5-S6 linkers) in slow inactivation of $hNa_V1.4$ and $hNa_V1.5$ sodium channels. In Fig. 1, portions of $hNa_V1.4$ channels are shown in blue and portions of $hNa_V1.5$ channels are shown in red, and resulting chimeras are designated as described in Materials and Methods.

Fig. 2 demonstrates steady-state slow inactivation in $hNa_V1.4$-$hNa_V1.5$ pore chimeras, plotted as normalized current amplitude versus 60-s prepulse voltage. The inset in Fig. 2 shows the pulse protocol used to measure steady-state slow inactivation. The data sets in Fig. 2 were fitted (solid lines) with a modified Boltzmann function (Eq. 2) to determine the probability of slow inactivation at depolarized voltages, midpoint ($V_{1/2}$) and slope factor (z). These results are summarized in Table 1. All panels in Fig. 2 also include fits to averaged steady-state slow inactivation data from $hNa_V1.4$ and $hNa_V1.5$ channels (dashed and dotted lines, respectively).

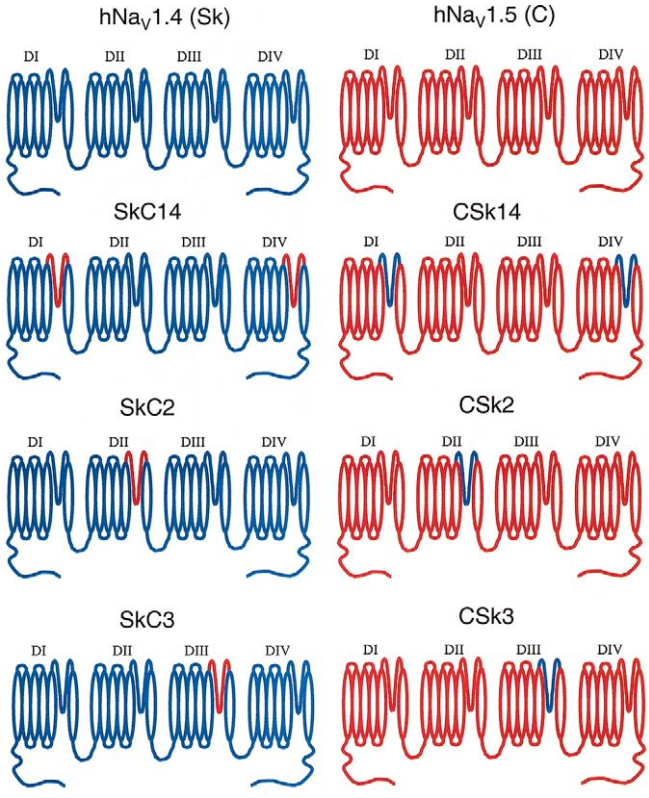

FIGURE 1 Schemes of $hNa_V1.4$-$hNa_V1.5$ pore chimeras.

The probability of slow inactivation in SkC14 in Fig. 2 *A* (filled circles, 80% ±3%, $n = 8$) is identical to $hNa_V1.4$ (dashed line, 84% ± 5%, $n = 10$, $p = 0.3$). The probability of slow inactivation in CSk14 in Fig. 2 *D* (open circles, 50% ± 4.1%, $n = 8$) is statistically identical to $hNa_V1.5$ channels (49% ± 3.6%, $n = 12$, $p = 0.9$). These results show that S5-S6 linkers in domains I and IV are not essential for controlling the probability of slow inactivation.

Fig. 2, *B* and *E*, demonstrate that domain II S5-S6 linkers, interchanged between $hNa_V1.4$ and $hNa_V1.5$ channels, statistically ($p \leq 0.0001$) affect the probability of slow inactivation relative to wild-type $hNa_V1.4$ and $hNa_V1.5$. In Fig. 2 *B* the probability in SkC2 reaches 52% (±4%, filled squares, $n = 8$) versus 84% ± 5% in $hNa_V1.4$. In Fig. 2 *E* the probability of slow inactivation in CSk2 is 73% (±4.1%, open squares, $n = 9$) versus 49% ± 3.6% in $hNa_V1.5$.

In contrast to the striking effect of transposing domain II p-regions, replacements of DIII S5-S6 linkers in SkC3 (Fig. 2 *C*, filled triangles) and in CSk3 (Fig. 2 *F*, open triangles) do not significantly change slow inactivation relative to $hNa_V1.4$ ($p = 0.1$) and $hNa_V1.5$ ($p = 1.0$). Thus, these results show that DII S5-S6 linkers, but not DI, DIII, or DIV S5-S6 linkers, strongly affect the probability of slow inactivation in both $hNa_V1.4$ and $hNa_V1.5$ sodium channels.

Data presented in Table 1 also demonstrate effects of interchanged p-regions on the midpoint ($V_{1/2}$) of steady-state slow inactivation. DII and DIII S5-S6 chimeras produce prominent effects on the midpoint ($p < 0.05$). $V_{1/2}$ value of steady-state inactivation for $hNa_V1.4$ is −81.3 mV (±4 mV, $n = 10$). SkC2 and SkC3 chimeras alter $V_{1/2}$ values of steady-state inactivation (−93.4 mV ± 1.7 mV, $n = 8$, and −56.4 mV ± 4.5 mV, $n = 9$, respectively). The $V_{1/2}$ values for CSk14 and CSk2 chimeras are not significantly different from that for $hNa_V1.5$ channels ($p \geq 0.05$).

The steady-state slow inactivation curves have different ($p = 0.01$) slope factors (z) in $hNa_V1.4$ and $hNa_V1.5$ sodium channels (−1.8 ± 0.2 vs. −0.8 ± 0.3, $n = 6$–10; Table 1), suggesting a different slow inactivation voltage sensitivity for these channels. Does a specific p-region also confer the voltage sensitivity of steady-state slow inactivation? We compared the z values of modified Boltzmann curves fit to steady-state slow inactivation data. Our results, summarized in Table 1, indicate that S5-S6 linkers do not equally or predictably contribute to the voltage sensitivity of steady-

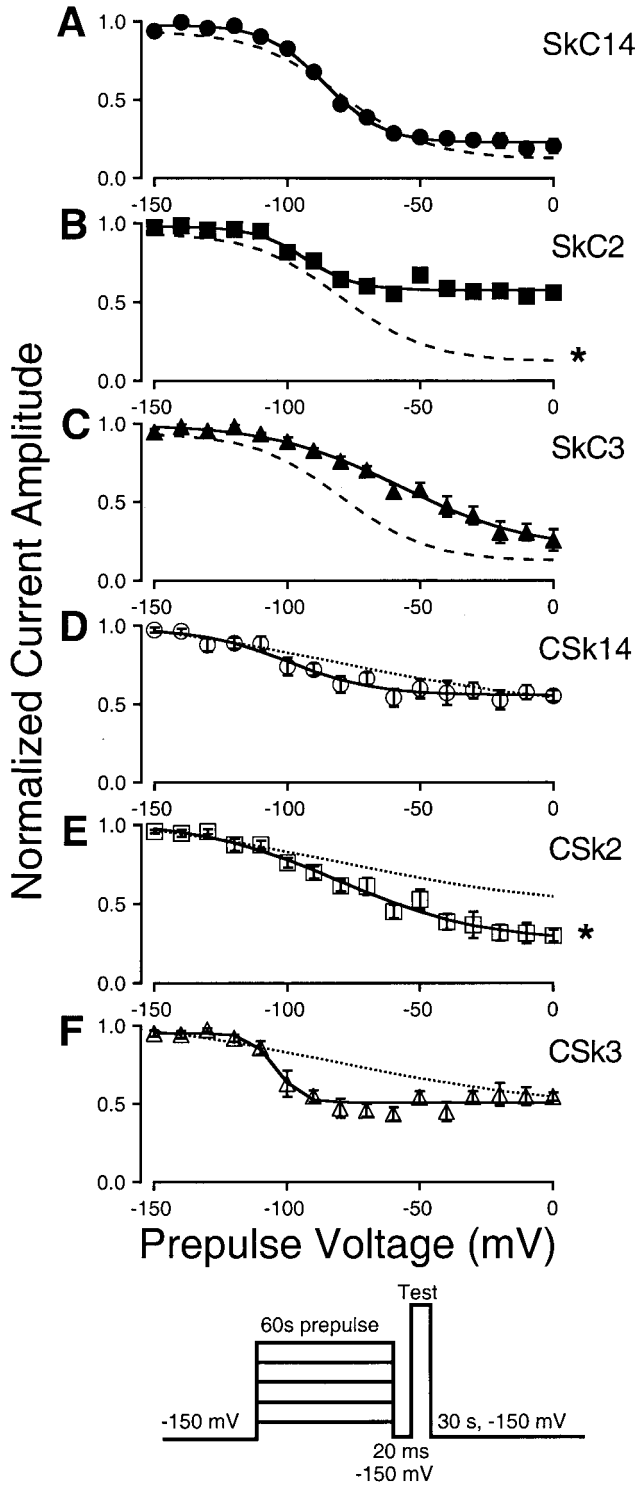

FIGURE 2 Alterations in domain DI-DIV pore regions lead to changes in slow inactivation in sodium channel chimeras. (*A–C*) Steady-state slow inactivation in SkC14 (●, $n = 8$), SkC2 (■, $n = 8$), and SkC3 (▲, $n = 9$), respectively; (*D–F*) Steady-state slow inactivation for CSk14 (○, $n = 8$), CSk2 (□, $n = 9$), and CSk3 (△, $n = 7$), respectively. In all graphs steady-state inactivation is plotted as average normalized current amplitude versus 60-s prepulse voltage. Mean ± SEM data were fitted with a modified Boltzmann function. Dotted lines represent modified Boltzmann fits to averaged steady-state slow inactivation probabilities in $hNa_V1.4$ ($A–C$) and $hNa_V1.5$ ($D–F$) sodium channels. Asterisks denote statistically significant differences in depolarized probabilities of slow inactivation in $hNa_V1.4$ compared with SkC2 ($p < 0.0001$) and slow inactivation in $hNa_V1.5$ compared with CSk2 sodium channels ($p < 0.0001$).

TABLE 1 Slow inactivation parameters for $hNa_V1.4$, $hNa_V1.5$, and $hNa_V1.4$-$hNa_V1.5$ chimeras

Channel	Level (%)	$V_{1/2}$ (mV)	Slope factor (z)
$hNa_V1.4$ (Sk)	84 ± 5 (10)	−81.3 ± 4 (10)	−1.8 ± 0.2 (10)
$hNa_V1.5$ (C)	49 ± 3.6 (12)*	−86.8 ± 15.3 (12)	−0.8 ± 0.3 (12)*
SkC14	80 ± 3 (8)	−84.5 ± 2.2 (8)	−1.8 ± 0.1 (8)
SkC2	52 ± 4 (8)*	−93.4 ± 1.7 (8)*	−1.7 ± 0.2 (8)
SkC3	78 ± 5 (9)	−56.4 ± 4.5 (9)*	−1.1 ± 0.2 (9)*
CSk14	50 ± 4.1 (8)	−94.6 ± 4 (8)	−1.3 ± 0.1 (8)
CSk2	73 ± 4.1 (9)†	−87.6 ± 4.3 (9)	−1 ± 0.1 (9)
CSk3	54 ± 3 (7)	−103.1 ± 2.5 (7)	−2.1 ± 0.2 (7)†
CP13	51 ± 3 (6)	−64.5 ± 6.3 (6)	−0.8 ± 0.1 (6)
CP15	48 ± 2 (4)	−90 ± 4.5 (4)	−1.2 ± 0.5 (4)
I891V	67 ± 7 (10)†	−75.7 ± 6.3 (10)	−1.1 ± 0.2 (6)
V754I	50 ± 4.5 (8)*	−80 ± 4.4 (8)	−1.1 ± 0.1 (8)
A773S/A776S	88 ± 5 (5)	−77.1 ± 7.4 (5)	−1.5 ± 0.2 (5)

Values of steady-state probabilities, $V_{1/2}$ and z for slow inactivation were obtained from Boltzmann fits to individual data sets (as described in Materials and Methods). Data are presented as means ± SEM.
*$P < 0.05$ versus $hNa_V1.4$.
†$P < 0.05$ versus $hNa_V1.5$.

state slow inactivation. Thus, slope factors were not significantly altered in chimeras SkC14 and SkC2 compared with $hNa_V1.4$ ($p > 0.05$). The slope factor in CSk3 chimera significantly ($p \leq 0.05$) differs from that of $hNa_V1.5$ channels (−2.1 ± 0.2, $n = 7$, vs. −0.8 ± 0.3, $n = 6$, respectively), whereas CSk14 and CSk2 chimeras have a significantly smaller effect on the voltage sensitivity ($p \geq 0.05$).

Site-directed mutations within the DII p-region alter the probability of steady-state slow inactivation in $hNa_V1.4$ and $hNa_V1.5$ channels

The DII S5-S6 linkers in $hNa_V1.4$ and $hNa_V1.5$ contain non-conserved regions and individual residues. We used chimerical constructs and site-directed mutagenesis to explore the ability of non-conserved residues to control the probability of slow inactivation. The structures of these chimeras are shown in Fig. 3.

We found that substitution of V754 in $hNa_V1.4$ with the corresponding isoleucine from $hNa_V1.5$ (V754I) significantly decreased the probability of slow inactivation from ~80% to ~50% ($p < 0.05$, $n = 6–10$). In Fig. 4 *A*, steady-state slow inactivation in V754I (filled circles, $n = 8$) is compared with that in $hNa_V1.5$ (dotted line, $n = 12$) and $hNa_V1.4$ channels (open circles, $n = 10$). The probability of slow inactivation in V754I is statistically indistinguishable from that in $hNa_V1.5$ channels ($p = 0.80$) but

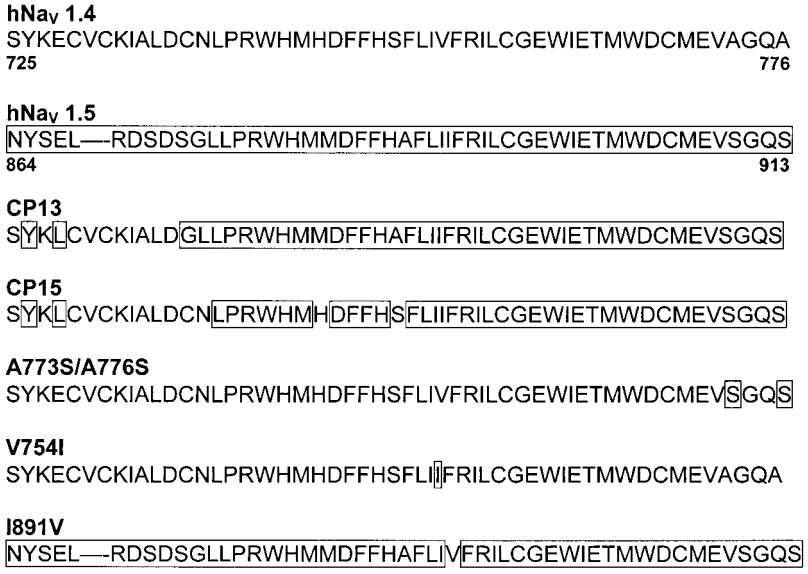

FIGURE 3 Structure of DII S5-S6 mutants. Residues contributed to the structure of hNaV1.4 DIIS5-S6 and hNaV1.5 DIIS5-S6 shown with plain and boxed symbols, respectively.

very different from hNa$_V$1.4 ($p < 0.001$). The reciprocal chimera in which I891 of hNa$_V$1.5 was replaced with the corresponding valine from hNa$_V$1.4 (I891V) also alters slow inactivation in hNa$_V$1.5. Because the I891V mutation appears to shift the steady-state curve in the depolarized direction, an extended range of prepulse voltages was applied (from −150 mV to 20 mV versus prepulse from −150 mV to 0 mV in other experiments). Fig. 4 *B* shows steady-state slow inactivation in I891V (filled squares, $n = 10$), hNa$_V$1.4 (dotted line, $n = 10$), and hNa$_V$1.5 channels (open squares, $n = 12$). Compared with hNa$_V$1.5 channels, I891V channels exhibit significantly ($p = 0.022$) increased probability of slow inactivation as determined from individual Boltzmann fits (49% ± 3.6% in hNa$_V$1.5, $n = 12$, vs. 67% ± 7% in I891V, $n = 10$). To estimate the effect of I891V on slow inactivation relative to hNa$_V$1.4, we compared probabilities of slow inactivation in I891V and hNa$_V$1.4 at prepulse voltages from −20 mV to 0 mV using the alternate Welch *t*-test for averaged sets of data with unequal standard deviations. The table in Fig. 4 *B* demonstrates that steady-state slow inactivation in I891V and hNa$_V$1.4 is similar at −20 mV and 0 mV ($p = 0.2$) and different at −10 mV ($p = 0.036$). By contrast, the CP13, CP15, and A777S/A776S chimeras do not alter the properties of steady-state slow inactivation (see Table 1).

Kinetics of slow inactivation in hNa$_V$1.4 and hNa$_V$1.5 channels are not dependent on the structure of p-regions

Do the S5-S6 extracellular linkers also confer the rates at which sodium channels enter and exit the slow inactivated state? To answer this question, we compared the voltage-dependent slow inactivation time constants of onset and recovery in wild-type and chimeric channels in Fig. 5, plotted as a function of prepulse voltage. The time constants were derived from single-exponential fits to slow inactivation recovery and onset data (see Vilin et al., 1999).

Exchange of S5-S6 linkers between hNa$_V$1.4 and hNa$_V$1.5 α-subunits produces neither a discernable pattern of alterations in voltage dependency of slow inactivation time constants [τ(V)] nor a consistent resemblance to the τ(V) characteristics of parental channels. Although most chimeras exhibit slow inactivation time constants (τ_s) different from those in wild-type channels at certain voltages (Fig. *B–F*), only τ_s in SCk14 chimera (Fig. 5 *A*) are obviously smaller than in hNa$_V$1.4 channels. τ_s in V754I (Fig. 6 *A*) and I891V (Fig. 6 *B*) channels remain similar to those in hNa$_V$1.4 and hNa$_V$1.5 channels.

DISCUSSION

Clarifying the molecular mechanisms underlying the divergent properties of slow inactivation in hNa$_V$1.4 and hNa$_V$1.5 will help elucidate the structure/function relations in these channels. We have previously demonstrated that replacing all p-regions in hNa$_V$1.4 α-subunit with the p-regions from hNa$_V$1.5 α-subunit brings the probability of slow inactivation in hNa$_V$1.4 to that in hNa$_V$1.5, indicating that the pore regions might underlie at least some of the inherent differences between hNa$_V$1.4 and hNa$_V$1.5 channels (Vilin et al., 1999). We have now systematically studied the role of single p-regions (S5-S6 linkers) from each domain of hNa$_V$1.4 and hNa$_V$1.5 α-subunits in regulating slow inactivation. Only the domain II S5-S6 linker was found to confer the probability of slow inactivation from parental channels into chimeric constructs (Fig. 2, *B* and *E*). S5-S6 linkers in domains DI, DIII, and DIV failed to significantly alter the probability slow inactivation compared with wild-type channels (Fig. 2, *A*, *C*, *D*, and *F*), showing

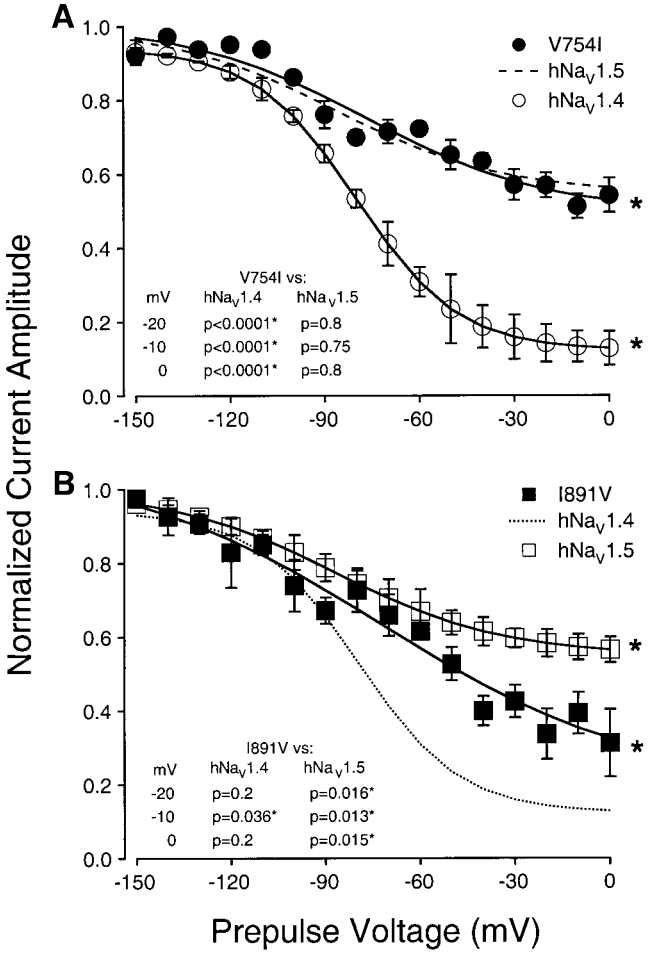

FIGURE 4 V754I and I891V mutations alter the steady-state probability of slow inactivation. (*A* and *B*) Steady-state slow inactivation in V754I (●, $n = 8$) and I891V (■, $n = 10$), respectively. Broken lines represent modified Boltzmann fits to averaged steady-state slow inactivation probabilities in $hNa_V1.5$ (*A*) and $hNa_V1.4$ (*B*) sodium channels. ○ and □, averaged steady-state slow inactivation data for $hNa_V1.4$ and $hNa_V1.5$, respectively. In all graphs, steady-state inactivation is plotted as average normalized current amplitude versus 60-s prepulse voltage. Mean ± SEM data were fitted with a modified Boltzmann function (——). The table in *A* compares steady-state inactivation in I891V versus $hNa_V1.4$ and $hNa_V1.5$ at voltages from −20 mV to 0 mV. The table in *B* compares steady-state inactivation in I891V versus $hNa_V1.4$ and $hNa_V1.5$ at voltages ranged from −20 mV to 0 mV. Asterisks denote statistically significant probabilities of steady-state slow inactivation in $hNa_V1.4$ compared with V754I ($p < 0.0001$) and slow inactivation in $hNa_V1.5$ compared with I891V sodium channels ($p = 0.02$).

that the p-regions in $hNa_V1.4$ and $hNa_V1.5$ channels do not have identical roles in slow inactivation. We further report the striking result that a single mutation, V754I, is capable of producing steady-state slow inactivation in $hNa_V1.4$ indistinguishable from that in $hNa_V1.5$ (Fig. 4 *A*). Isoleucine 891 in $hNa_V1.5$ DII S5-S6, corresponding to V751 in $hNa_V1.4$, produces a similar effect on steady-state slow inactivation (Fig. 4 *B*), although we find that the lower plateau of steady-state slow inactivation in $hNa_V1.5$ I891V is shifted to more depolarized potentials. From these results, it appears that V754 and I891 are essential for determining the difference in probability of slow inactivation between cardiac and skeletal muscle sodium channels.

In contrast to the relatively clear role of the DII p-region in regulating the probability of slow inactivation, effects of single S5-S6 linkers on slow inactivation time constants are less easily interpreted. SkC2, V754I, and I891V chimeras most closely resemble slow inactivation time constants of those in $hNa_V1.4$ and $hNa_V1.5$ channels (Figs. 5 *B* and Fig. 6), whereas all other pore chimeras have generally smaller slow inactivation time constants, compared with $hNa_V1.4$ and $hNa_V1.5$ channels (Fig. 5), especially for SkC14 (Fig. 5 *A*). The lack of a clear correlation between the structure of p-regions and slow inactivation time constants suggests that the S5-S6 linkers of $hNa_V1.4$ and $hNa_V1.5$ do not directly determine the voltage-dependent rates of slow inactivation. According to the results shown in Fig. 5, it is plausible that the kinetic properties of slow inactivation in sodium channels do not arise from the structure of the p-regions, but rather may be dependent on other voltage-sensitive structures, such as the S4 transmembrane segments, as has been proposed elsewhere (Kontis and Goldin, 1997). The absence of a predictable relationship between the steady-state probability and the kinetics of slow inactivation is further complicated by the previous observation that slow inactivation cannot be adequately described using a simple, two-state model (Featherstone et al., 1996).

Our results are consistent with other reports showing that p-regions are involved in slow inactivation gating in sodium channels. First, structural alterations within sodium channel p-regions and their close proximity affect slow inactivation (Cummins and Sigworth, 1996; Hayward et al., 1997; Wang and Wang, 1997). Second, changes in ionic environment affect slow inactivation in sodium channels; low external $[Na^+]$ accelerates entry into the slow inactivated state, slows the rate of recovery from slow inactivation, and increases the probability of slow inactivation (Townsend and Horn, 1997). These data suggest that the sodium channel p-regions may have dual roles as both the conductance pore (Catterall, 1993, Fozzard and Hanck, 1996; Marban et al., 1998) and as the slow inactivation gate.

In addition to the p-regions, other sodium channel structures have also been shown to affect slow inactivation in sodium channels, indicating that slow inactivation gating is realized through complex, voltage-dependent interactions between disparate structures. The domain III-IV cytoplasmic linker, responsible for fast inactivation in sodium channels (West et al., 1992; Patton et al., 1994) has been demonstrated to limit the probability of slow inactivation in both cardiac (Richmond et al., 1998) and skeletal muscle channels (Featherstone et al., 1996). We have also shown preliminary evidence that substitution of glutamate 1314 with glutamine in the DIII-IV linker decreases the probability of slow inactivation in $hNa_V1.4$ channels (Spackman et al.,

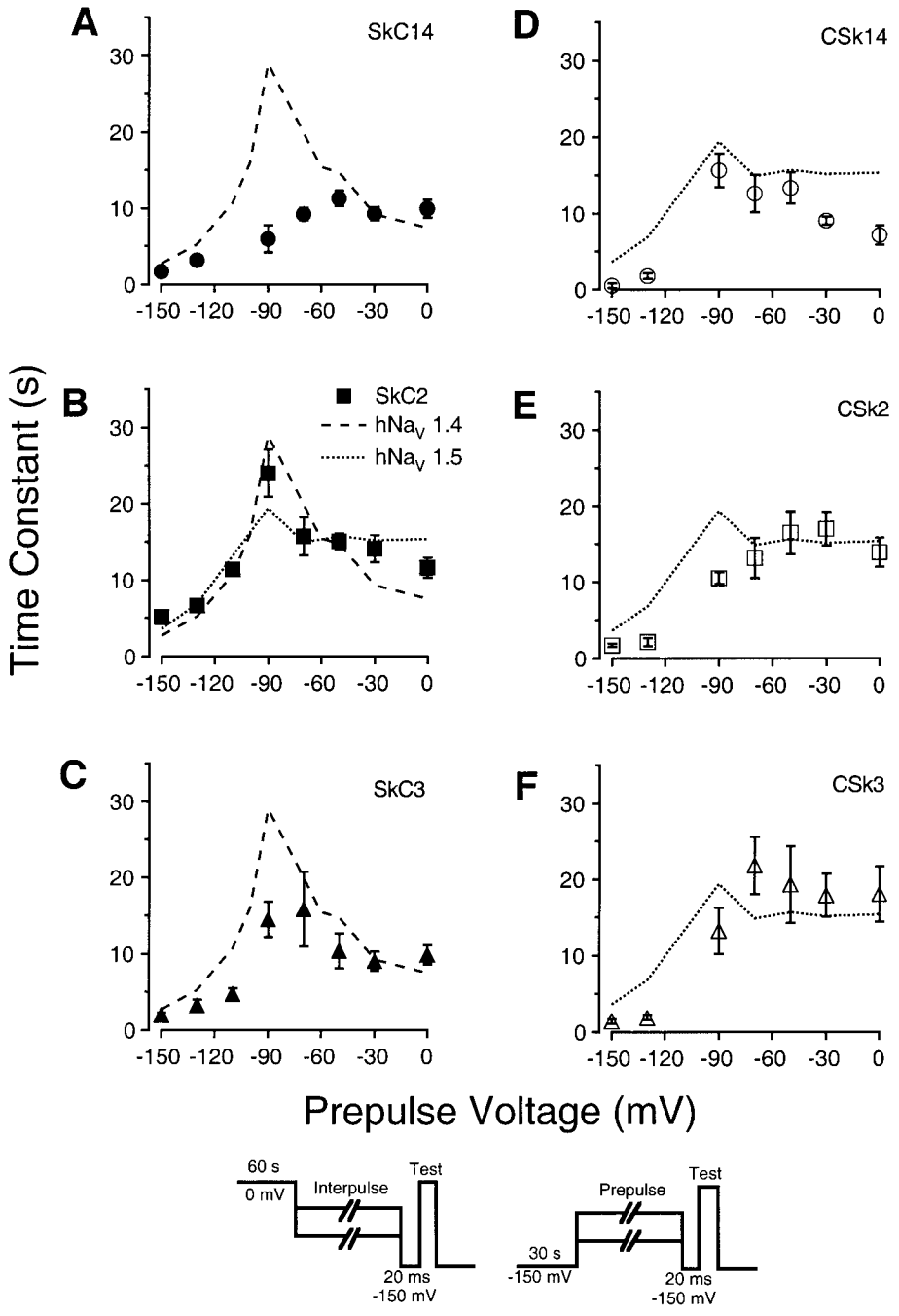

FIGURE 5 Interchanged p-regions accelerate slow inactivation time constants in hNa$_V$1.4-hNa$_V$1.5 pore chimeras. (*A–C*) Averaged time constants for slow inactivation in SkC14 (●, $n = 5–8$), SkC2 (■, $n = 4–7$), and SkC3 (▲, $n = 4–7$), respectively. (*D–F*) Averaged time constants for slow inactivation in CSk14 (○, $n = 4–7$), CSk2 (□, $n = 5–12$), and CSk3 (△, $n = 5–7$), respectively. Time constants derived from single-exponential fits to slow inactivation recovery and slow inactivation onset data (not shown) obtained using the set of protocols as shown at the bottom. In all graphs the slow inactivation time constants are plotted versus 60-s prepulse voltage. Broken lines represent the averaged slow inactivation time constants in hNa$_V$1.4 (*A–C*) and hNa$_V$1.5 (*D–F*) sodium channels. All values represent mean ± SEM.

2000). In addition, the role of S4 voltage sensors in sodium channel slow inactivation gating has been hypothesized (Bezanilla et al., 1982; Rayner and Starkus 1989; Ruben et al., 1992) and experimentally confirmed (Kontis and Goldin, 1997; Mitrovic et al., 2000).

The pore-forming structures and S4 segments are important components underlying slow C- and P-type inactivation in *Shaker* K^+ channels (Hoshi et al., 1990; Yellen et al., 1994; Liu et al., 1996; Kiss et al., 1999, Loots and Isacoff, 2000). Certain point mutations in the K^+ channel pore region block the potassium current and affect slow inactivation, additionally indicating that at least the outer pore of potassium channels is also functioning as slow inactivation gates (Yang et al., 1997b; Yellen et al., 1994; Liu et al., 1996). In contrast to the ball-and-chain mechanism of N-type inactivation (Hoshi et al., 1991), C- and P-type inactivation is produced by pore occlusion via a series of movements within the p-region (Boland et al., 1994; Liu et al., 1996; Cha and Bezanilla, 1997), which are presumably driven by the S4 voltage sensors (Loots and Isacoff, 1999, 2000).

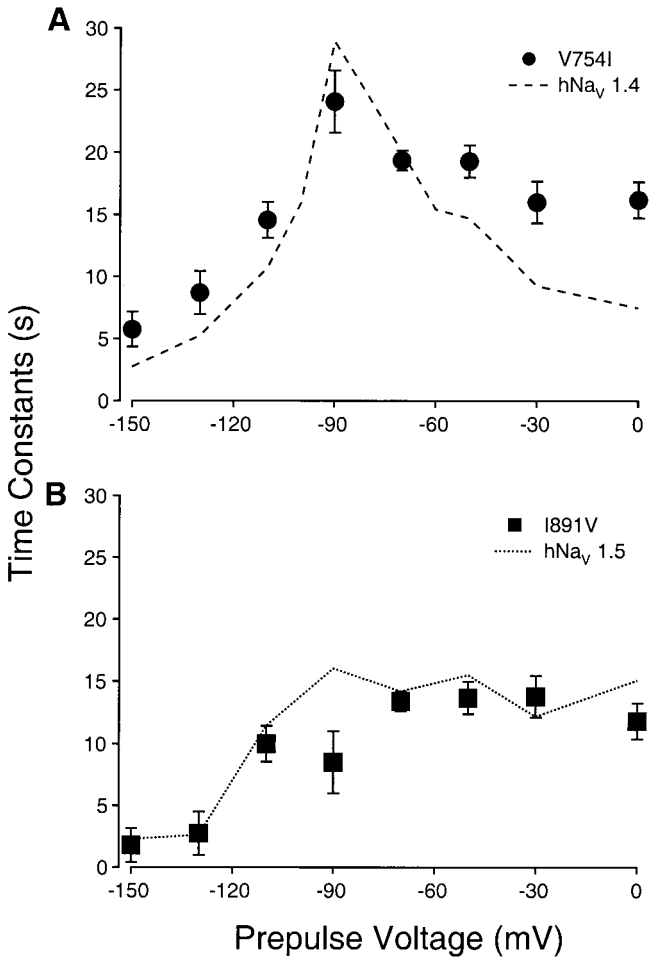

FIGURE 6 Voltage dependency of slow inactivation time constants in V754I and I891V channels. (*A* and *B*) Averaged time constants for slow inactivation in V754I (●, $n = 6–8$) and I891V (■, $n = 5–7$), respectively. Time constants derived from single-exponential fits to slow inactivation recovery and slow inactivation onset data (not shown) were obtained using the set of protocols as shown in Fig. 5. In all graphs the slow inactivation time constants are plotted versus 60-s prepulse voltage. Broken lines represent the averaged slow inactivation time constants in hNa$_V$1.4 (*A*) and hNa$_V$1.5 (*B*) sodium channels. All values represent mean ± SEM.

It seems that slow inactivation in sodium channels is also produced by conformational changes in the α-subunit through the combined movement of S4 voltage sensors and p-regions. It is easy to imagine that movements within the p-regions could convert the channel into a non-conducting state and reduce the number of available channels during a 60-s depolarizing pulse (Ruff, 1996; Townsend and Horn, 1997). Consequently, the probability of slow inactivation might be determined by the greater (in hNa$_V$1.4) or lesser (in hNa$_V$1.5) flexibility or mobility of a particular p-region, or differential interactions between the pore and the other channel structures that directly or indirectly control slow inactivation. This speculation is supported by the observation that exchanging the DII S5-S6 linker between two channel isoforms confers the parental channel properties of steady-state slow inactivation into the chimeric construct (Fig. 2, *B* and *E*). Our observation that a single residue within the DII S5-S6 region regulates the steady-state probability of slow inactivation in hNa$_V$1.4 and hNa$_V$1.5 channels (Fig. 4) is also consistent with this idea.

Our data do not provide any evidence that p-regions are directly involved in the regulation of slow inactivation time constants, but rather suggest that other voltage-dependent structures play a role in this process. It was recently demonstrated that covalent binding of sodium (2-sulfonatoethyl)methanethiosulfonate to a cysteine, substituted for the third arginine in the domain IV S4 voltage sensor, increases the rate of entering the slow inactivated state at depolarized voltages and decreases the rate of leaving this state at hyperpolarized voltages (Mitrovic et al., 2000). These data show that S4 voltage sensors, or at least the S4 segment from the domain IV, can affect the kinetics of slow inactivation in sodium channels. Additionally, we have shown preliminary data that charge neutralizations (R219C and K228C) in the DI S4 segment alter the apparent voltage dependence of steady-state slow inactivation (Vilin et al., 2000). Thus, because the DIV S4 voltage sensor participates in coupling both activation and deactivation with fast inactivation (Ji et al., 1996; Cha et al., 1999; Groome et al., 1999, 2000; Sheets et al., 2000), the role of the S4s in slow inactivation is particularly interesting as a possible mechanism of coupling between fast and slow gating transitions.

We are grateful to Drs. Brett Adams and Tim Gilbertson for their editorial comments on the manuscript.

This work was supported by U.S. Public Health Service grant NS29204 to P.C.R.

REFERENCES

Armstrong, C. M., and F. Bezanilla. 1977. Inactivation of the sodium channel. II. Gating current experiments. *J. Gen. Physiol.* 70:567–590.

Bezanilla, F., R. E. Taylor, and J. M. Fernandez. 1982. Distribution and kinetics of membrane dielectric polarization. I. Long-term inactivation of gating currents. *J. Gen. Physiol.* 79:21–40.

Boland, L. M., M. E. Jurman, and G. Yellen. 1994. Cysteines in the *Shaker* K^+ channels are not essential for channel activity or zinc modulation. *Biophys. J.* 66:694–699.

Cannon, S. C., A. I. McClatchey, and J. F. Gusella. 1993. Modification of Na^+ current conducted by the rat skeletal muscle α subunit by co-expression with a human brain β subunit. *Pflügers Arch.* 423:155–157.

Catterall, W. A. 1993. Structure and function of voltage-gated ion channels. *Trends Neurosci.* 16:500–506.

Cha, A., and F. Bezanilla. 1997. Characterizing voltage-dependent conformational changes in the *Shaker* K^+ channel with fluorescence. *Neuron.* 19:1127–1140.

Cha, A., P. C. Ruben, A. L. George, Jr., E. Fujimoto, and F. Bezanilla. 1999. Voltage sensors in domains III and IV, but not I and II, are immobilized by Na^+ channel fast inactivation. *Neuron.* 22:73–87.

Chandler, W. K., and H. Meves. 1970. Slow changes in membrane permeability and long-lasting action potentials in axons perfused with sodium fluoride. *J. Physiol. (Lond.).* 211:707–728.

Chen, C., and S. C. Cannon. 1995. Modulation of Na^+ channel inactivation by the β-subunit: a deletion analysis. *Pflügers Arch.* 431:186–195.

Cummins, T. R., and F. J. Sigworth. 1996. Impaired slow inactivation in mutant sodium channels. *Biophys. J.* 71:227–236.

Featherstone, D. E., J. E. Richmond, and P. C. Ruben. 1996. Interaction between fast and slow inactivation in Skm1 sodium channels. *Biophys. J.* 71:3098–3109.

Fleidervish, I. A., A. Freidman, and M. J. Gutnick. 1996. Slow inactivation of Na^+ current and slow cumulative spike adaptation in mouse and guinea pig neocortical neurones in slices. *J. Physiol. (Lond.).* 493:83–97.

Fozzard, H. A., and D. A. Hanck. 1996. Structure and function of voltage-dependent sodium channels: comparison of brain II and cardiac isoforms. *Physiol. Rev.* 76:887–926.

Gellens, M. E., A. L. George, J. Chen, L. Q. Chahine, M. Horn, R. L. Barchi, and R. G. Kallen. 1992. Primary structure and functional expression of the human cardiac tetrodotoxin-insensitive voltage-dependent sodium channels. *Proc. Natl. Acad. Sci. U.S.A.* 89:554–558.

George, A. L., J. Komisarof, R. G. Kallen, and R. L. Barchi. 1992. Primary structure of the adult human skeletal muscle voltage-dependent sodium channels. *Ann. Neurol.* 31:131–137.

Goldin, A. L., R. L. Barchi, J. H. Caldwell, F. Hofmann, J. R. Howe, J. C. Hunter, R. G. Kallen, et al. 2000. Nomenclature of voltage-gated sodium channels. *Neuron.* 28:365–368.

Groome, J. R., E. Fujimoto, A. L. George, Jr., and P. C. Ruben. 1999. Differential effects of homologous S4 mutations in human skeletal muscle sodium channels on deactivation gating from open and inactivated states. *J. Physiol.* 516:687–698.

Groome, J. R., E. Fujimoto, and P. C. Ruben. 2000. The delay in recovery from fast inactivation in skeletal muscle sodium channels is deactivation. *Cell. Mol. Neurobiol.* 20:521–527.

Hartmann, H. A., A. A. Tiedman, S. F. Chen, A. M. Brown, and G. E. Kirsch. 1994. Effects of III-IV linker mutations on human heart Na^+ channel inactivation gating. *Circ. Res.* 75:114–122.

Hayward, L. J., R. H. Brown, and S. C. Cannon. 1997. Slow inactivation differs among mutant Na channels associated with myotonia and periodic paralysis. *Biophys. J.* 72:1204–1219.

Hille, B. 1992. Ionic Channels of Excitable Membranes. Sinauer Associates, Sunderland, MA.

Ho, H. N., H. D. Hunt, R. M. Morton, J. K. Pullen, and L. R. Pease. 1989. Site-directed mutagenesis by overlap extension using the polymerase chain reaction. *Gene.* 77:51–59.

Hoshi, T., W. N. Zagota, and R. W. Aldrich. 1990. Biophysical and molecular mechanisms of *Shaker* potassium channel inactivation. *Science.* 250:533–538.

Hoshi, T., W. N. Zagota, and R. W. Aldrich. 1991. Two types of inactivation in *Shaker* K^+ channels: effects of alterations in the carboxy-terminal region. *Neuron.* 7:547–556.

Isom, L. L., K. S. De Jongh, and W. Catterall. 1994. Auxiliary subunits of voltage-gated ion channels. *Neuron.* 12:1183–1194.

Isom, L. L., K. S. De Jongh, D. E. Patton, B. F. X. Reber, J. Offord, H. Charbonneau, K. Walsh, A. L. Goldin, and W. A. Catterall. 1992. Primary structure and functional expression of the β_1 subunit of the rat brain sodium channel. *Science.* 256:839–842.

Ji, S., A. L. George, Jr., R. Horn, and R. L. Barchi. 1996. Paramyotonia congenita mutations reveal different roles for segments S3 and S4 of domain D4 in hSkM1 sodium channel gating. *J. Gen. Physiol.* 107: 183–194.

Kiss, L., J. LoTurco, and S. J. Korn. 1999. Contribution of the selectivity filter to inactivation in potassium channels. *Biophys. J.* 76:253–263.

Kontis, K., and A. Goldin. 1997. Sodium channel inactivation is altered by substitution of voltage sensor positive charges. *J. Gen. Physiol.* 110: 403–413.

Loots, E., and E. Y. Isacoff. 1999. Protein rearrangements underlying slow inactivation of the *Shaker* K^+ channel. *J. Gen. Physiol.* 112:377–389.

Loots, E., and E. Y. Isacoff. 2000. Molecular coupling of S4 to a K^+ channel's slow inactivation gate. *J. Gen. Physiol.* 116:623–635.

Liu, Y., M. E. Jurman, and G. Yellen. 1996. Dynamic rearrangement of the outer mouth of a K^+ channel during gating. *Neuron.* 16:859–867.

Makita, N., P. B. Bennett, and A. L. George. 1994. Voltage-gated Na^+ channels β_1 subunit mRNA expressed in adult human skeletal muscle, heart, and brain is encoded by a single gene. *J. Biol. Chem.* 269: 7571–7578.

Makita, N., P. B. Bennett, and A. L. George. 1996. Molecular determinants of β_1 subunit induced gating modulation in voltage-dependent Na^+ channels. *J. Neurosci.* 16:7117–7127.

Marban, E., T. Yamagishi, and G. Tomaselli. 1998. Structure and function of voltage-gated sodium channels. *J. Physiol. (Lond.).* 508:647–657.

McCormick, K. A., L. L. Isom, D. Ragsdale, D. Smith, T. Scheuer, and W. A. Catterall. 1998. Molecular determinants of Na^+ channel function in the extracellular domain of the β_1 subunit. *J. Biol. Chem.* 273: 3954–3962.

Mitrovic, N., A. L. George, Jr., and R. Horn. 2000. Role of domain IV in sodium channel slow inactivation. *J. Gen. Physiol.* 115:707–717.

O'Reilly, J. P., S. Y. Wang, R. G. Kallen, and G. K. Wang. 1999. Comparison of slow inactivation in human heart and rat skeletal muscle in Na^+ chimeras. *J. Physiol. (Lond.).* 515:61–73.

Patton, D. E., L. L. Isom, W. A. Catterall, and A. L. Goldin. 1994. The adult rat β_1 subunit modifies activation and inactivation gating of multiple sodium channel α subunit. *J. Biol. Chem.* 269:17649–17655.

Patton, D. E., J. W. West, W. A. Caterall, and A. L. Goldin. 1992. Amino acids residues required for fast sodium channel inactivation: charge neutralization and deletions in the III-IV linker. *Proc. Natl. Acad. Sci. U.S.A.* 89:10905–10909.

Rayner, M. D., and J. G. Starkus. 1989. The steady-state distribution of gating charge in crayfish giant axons. *Biophys. J.* 58:1169–1181.

Richmond, J. E., D. E. Featherstone, H. A. Hartmann, and P. C. Ruben. 1998. Slow inactivation in human cardiac sodium channels. *Biophys. J.* 74:2945–2952.

Rogart, R. B., L. L. Crebbs, L. K. Muglia, D. D. Kephart, and M. W. Kaiser. 1989. Molecular cloning of a putative tetrodotoxin-resistant rat heart Na^+ channel isoform. *Proc. Natl. Acad. Sci. U.S.A.* 86: 8170–8174.

Ruben, P. C., J. G. Starkus, and M. D. Rayner. 1992. Steady-state availability of sodium channels: interactions between activation and slow inactivation. *Biophys. J.* 61:941–955.

Rudy, B. 1978. Slow inactivation of the sodium conductance in squid giant axons: pronase resistance. *J. Physiol. (Lond.).* 283:1–21.

Ruff, R. L. 1996. Single-channel basis of slow inactivation of Na^+ channels in rat skeletal muscle. *Am. J. Physiol.* 271:C971–C981.

Ruff, R. L., L. Simoncini, and W. Stühmer. 1988. Slow sodium channel inactivation in mammalian muscle: a possible role in regulating excitability. *Muscle Nerve.* 11:502–510.

Sato, C., M. Sato, A. Iwasaki, T. Doi, and A. Engel. 1998. The sodium channel has four domains surrounding a central pore. *J. Struct. Biol.* 121:314–325.

Salgado, V. L., J. Z. Yeh, and T. Narahashi. 1985. Voltage-dependent removal of sodium inactivation by N-bromoacetamide and pronase. *Biophys. J.* 47:567–571.

Starkus, J. G., and P. Shrager. 1978. Modification of slow sodium inactivation in nerve after internal perfusion with trypsin. *Am. J. Physiol.* 4:C238–C244.

Sawczuk, A., R. K. Powers, and M. D. Binder. 1995. Spike frequency adaptation studied in hypoglossal motoneurons of the rat. *J. Neurophysiol.* 73:1799–1810.

Sheets, M. F., J. W. Kyle, and D. A. Hanck. 2000. The role of the putative inactivation lid in sodium channel gating current immobilization. *J. Gen. Physiol.* 115:609–619.

Spackman, S., E. Fujimoto, Y. Y. Vilin, and P. C. Ruben. 2000. Charged residues in the DIII-DIV linker control the level of steady-state slow inactivation in sodium channels. *Biophys. J.* 78:A497.

Toib, A., V. Lyakhov, and S. Marom. 1998. Interaction between duration of activity and time course of recovery from slow inactivation in mammalian brain Na^+ channels. *J. Neurosci.* 18:1893–1903.

Townsend, C., and R. Horn. 1997. Effect of alkali metal cations on slow inactivation of cardiac Na^+ channels. *J. Gen. Physiol.* 110:23–33.

Trimmer, J. S., S. S. Cooperman, S. A. Tomiko, J. Zhou, S. M. Crean, M. B. Boyle, R. G. Kallen, Z. Sheng, R. L. Barchi, F. J. Sigworth, R. H. Goodman, W. S. Agnew, and G. Mandel. 1989. Primary structure and

functional expression of a mammalian skeletal muscle sodium channel. *Neuron.* 3:33–49.

Valenzuela, C., and P. B. Bennett. 1994. Gating of cardiac Na^+ channels in excised membrane patches after modification by α-chymotrypsin. *Biophys. J.* 67:161–171.

Vedantham, V., and S. C. Cannon. 1998. Slow inactivation does not affect movement of the fast inactivation gate in voltage-gated Na^+ channels. *J. Gen. Physiol.* 111:83–93.

Vilin, Y. Y., E. Fujimoto, J. Repscher, A. L. George, N. Makita, and P. C. Ruben. 2000. Mechanisms of slow inactivation in human skeletal muscle and human cardiac sodium channels. *Biophys. J.* 78:A488.

Vilin, Y. Y., N. Makita, A. L. George, and P. C. Ruben. 1999. Structural determinants of slow inactivation in human cardiac and skeletal muscle sodium channels. *Biophys. J.* 77:1384–1393.

Wang, S. Y., and G. K. Wang. 1997. A mutation in segment I-S6 alters slow inactivation of sodium channels. *Biophys. J.* 72:1633–1640.

West, J. W., D. E. Patton, T. Scheuer, Y. Wang, A. L. Goldin, and W. A. Catterall. 1992. A cluster of hydrophobic amino acid residues required for fast Na^+-channel inactivation. *Proc. Natl. Acad. Sci. U.S.A.* 89: 10910–10914.

Yang, J. S., P. B. Bennett, N. Makita, A. L. George, and R. L. Barchi. 1993. Expression of the sodium channel β-subunit in rat skeletal muscle is selectively associated with the tetrodotoxin-sensitive α-subunit isoform. *Neuron.* 11:915–922.

Yang, N., A. L. George, Jr., and R. Horn. 1997a. Probing the outer vestibule of a sodium channel voltage sensor. *Biophys. J.* 73:2260–2268.

Yang, Y., Y. Yan, and F. J. Sigworth. 1997b. How does the W434F mutation block current in *Shaker* potassium channels? *J. Gen. Physiol.* 109:779–789.

Yellen, G., D. Sodickson, T. Y. Chen, and M. E. Jurman. 1994. An engineered cysteine in the external mouth of a K^+ channel allows inactivation to be modulated by metal binding. *Biophys. J.* 66: 1068–1075.